European Journal of Medicinal Chemistry 45 (2010) 5438–5451

Contents lists available at ScienceDirect

European Journal of Medicinal Chemistry

journal homepage: http://www.elsevier.com/locate/ejmech

Original article

In vivo and *in vitro* evaluation of highly specific thiolate carrier group copper(II) and zinc(II) complexes on Ehrlich ascites carcinoma tumor model

N. Raman [a,*], R. Jeyamurugan [a], R. Senthilkumar [b], B. Rajkapoor [c], Scott G. Franzblau [d]

[a] Research Department of Chemistry, VHNSN College, Virudhunagar-626 001, Tamil Nadu, India
[b] Department of Pharmaceutical Chemistry, Swami Vivekanandha College of Pharmacy, Elayampalayam, Tiruchengodu-637 205, Tamil Nadu, India
[c] Department of Pharmacology, Sebha University, Sebha, Libya
[d] Institute for Tuberculosis Research, College of Pharmacy, University of Illinois, Chicago, IL 60612-723, USA

ARTICLE INFO

Article history:
Received 10 June 2010
Received in revised form
30 August 2010
Accepted 1 September 2010
Available online 15 September 2010

Keywords:
DNA binding
Nuclease activity
Antitumor activity
Benzene dithiolate complexes
Ehrlich ascites carcinoma
Human cancer cell lines
H37Rv strain

ABSTRACT

A new series of copper(II) and zinc(II) complexes have been designed and synthesized using a new type of Schiff bases derived from the reaction of 3-(3-phenyl-allylidene)-pentane-2,4-dione with *para* substituted aniline and benzene-1,2-dithiol. Their structures have been established by analytical and spectral data. The higher ε and low $A_{\|}$ values together with positive reduction potentials for these copper complexes suggest that they can mimic the functional properties of naturally occurring proteins. *In vivo* and *in vitro* antitumor functions of the complexes against Ehrlich ascites carcinoma tumor model have been investigated. The minimum inhibitory concentration of the complexes has also been investigated against *Mycobacterium tuberculosis* strain H37Rv. These complexes exhibit significant antitumor, cytotoxic and antituberculosis activity.

1. Introduction

The better understanding of both the chemical properties and the pharmacological action of cisplatin has guided the development of analogs having always *cis* geometry but differing from cisplatin either for the ammine carrier ligands or for the leaving chlorides. In general, modification of the chloride leaving groups of cisplatin results in compounds with different pharmacokinetic properties, whereas modification of the carrier ligands alters the efficacy and/or the spectrum of activity of the resulting complex. Thousands of platinum compounds have been synthesized and screened for their antitumor activity, but little success has been achieved so far in finding novel platinum-based drugs active towards cisplatin resistant/refractory tumors [1,2]. Pt(II) has a strong thermodynamic preference for binding to S-donor ligands. For that reason, one would predict that platinum compounds would perhaps never reach DNA, with many cellular platinophiles (S-donor ligands, such as glutathione, methionine) as competing ligands in the cytosol [3,4]. Despite the success of cisplatin, however, it lacks selectivity for tumor tissue, which leads to severe side effects. These include renal impairment, neurotoxicity and ototoxicity (loss of balance/hearing), which are only partially reversible when the treatment is stopped. With long-term or high-dose therapy, severe anemia may develop [5,6]. To address these problems, modified versions of cisplatin, leading to second and third generation platinum-based drugs have been synthesized over the past 30 years. Several platinum complexes are currently in clinical trials, but some of these new complexes have not yet demonstrated such significant advantages over cisplatin.

With the exception of platinum(II) compounds, there is relatively little mechanistic information on how metal anti-cancer drugs function, but it is clear that metal ions can work by a variety of different routes. Non-platinum active compounds are likely to have mechanism of action, biodistribution and toxicity which are different from those of platinum drugs and might be effective against human cancers that are poor chemosensitive or have become resistant to conventional platinum drugs. Among the different therapeutic strategies to eradicate cancer cells through DNA damage, the view of using transition metal complexes, capable of oxidative or hydrolytic DNA cleavage as anti-cancer drugs, is a challenging topic in bioinorganic chemistry [7,8].

In the last few decades, interest in the study of metal–thiolates has ensued as a result of the following factors [9–15]: (i) Thiolates reduce

* Corresponding author. Tel.: +91 092451 65958; fax: +91 4562 281338.
E-mail address: drn_raman@yahoo.co.in (N. Raman).

0223-5234/$ – see front matter © 2010 Elsevier Masson SAS. All rights reserved.
doi:10.1016/j.ejmech.2010.09.004

the toxic effect of soft heavy metals such as Cd, Hg and Pb. (ii) Thiolate donors are present in the coordination sphere of metal ions in active sites of metalloproteins [16]; *e.g*, Fe(II) in peptide deformylase [17], Co (II) in the active site of nitrile hydratase [18], [NiFe]-hydrogenase [19] and metallothioneins containing Zn, Hg, Cd, and Cu [20]. (iii) In the application of certain metal–thiolates in medicine, such as Au(I)-thiolates for the treatment of arthritis and triphenylphosphinegold(I) compounds as antitumor agents [21]. Recently technetium– and rhenium–thiolates have gained importance in medical radiotherapeutic applications [22]. (iv) Metal–thiolates are known to be involved in radioactive protective efficacy and protection against alkylating reagents. These metal complexes contribute to a greater capacity to scavenge the superoxide radicals produced on exposure to ionizing radiation [23,24].

This inspires for developing new non-platinum anti-cancer agents which include the incorporation of carrier groups that can target tumor cells with high specificity. Hence, we have a strategy to modify the previously reported [25] cisplatin based copper(II) and zinc(II) complexes using benzene-1,2-dithiol. One of the main reasons for this adaptation is that the soft metals are strongly bonded with soft bases like thiolate. This type of adaptation may arise due to the slower intracellular hydrolysis of thiolate ligands compared to the monodentate chloro ligands of cisplatin. This amendment may reduce the toxicity in intracellular metabolism compared to cisplatin. Bearing these facts in mind, it is planned to synthesize and characterize new copper(II) and zinc(II) complexes of the above type and to investigate the *in vivo* and *in vitro* antitumor activity of the synthesized complexes against Ehrlich ascites carcinoma (EAC) tumor model.

2. Chemistry

The starting Knoevenagel condensate Schiff base ligands were prepared as described in the literature procedure [25], by the condensation of 3-(3-phenyl-allylidene)-pentane-2,4-dione with *para* substituted aniline(X); X = $-NO_2$ (L^1), $-H$ (L^2), $-OH$ (L^3) and $-OCH_3$ (L^4). They were refluxed with copper(II)/zinc(II) chloride to form [$MLCl_2$] type complexes. The labile chlorine atom was replaced by benzene-1,2-dithiolate ligand (bdt) to form [ML(bdt)] type complexes. Synthetic route for the preparation of complexes is depicted in Scheme 1. The synthesized ligands and their complexes were stable to air and moisture. The ligands were soluble in common organic solvents but their complexes were soluble only in DMF and DMSO. The synthesized ligands were characterized by the usual spectral and analytical techniques. The complexes were found to be 1:1 electrolytic nature in 10^{-3} M DMF solution, implying the non-coordination of chloride anion to the central metal ion. The absence of counter (chloride) ion was confirmed from Volhard's test. The elemental analysis results for the metal complexes were also agreed with the calculated values showing that the complexes have 1:1 metal/ligand ratio. The analytical data, conductivity and magnetic moment of the complexes are given along with their synthetic procedures.

3. Pharmacology

The DNA binding study of the synthesized complexes with CT DNA was carried out by electronic absorption spectroscopy, viscosity measurements, cyclic voltammetry and differential pulse voltammetry. Gel electrophoresis experiments using pUC19 circular plasmid DNA were performed with the ligands and their complexes in the presence and absence of H_2O_2 as an oxidant. The nuclease activity of the complexes was also investigated in the presence of a free radical scavenger, dimethylsulfoxide (DMSO) and singlet oxygen quencher, azide ion (NaN_3). A detailed understanding of the structural and electronic properties of drug–DNA complexes and their mechanism of binding is the key step in elucidating the principles of their anti-cancer activity. *In vivo* and *in vitro* antitumor functions of synthesized complexes against Ehrlich ascites carcinoma (EAC) tumor model were investigated. The antitumor activity was assessed by hematological parameters, median survival time and cell viability with trypan blue dye exclusion assay. *In vitro* antitumor activity was performed by MTT assay against human cervical cancer cell lines (HeLa), Human laryngeal epithelial cancer (Hep2), Human liver cancer (HepG2) and Human breast cancer

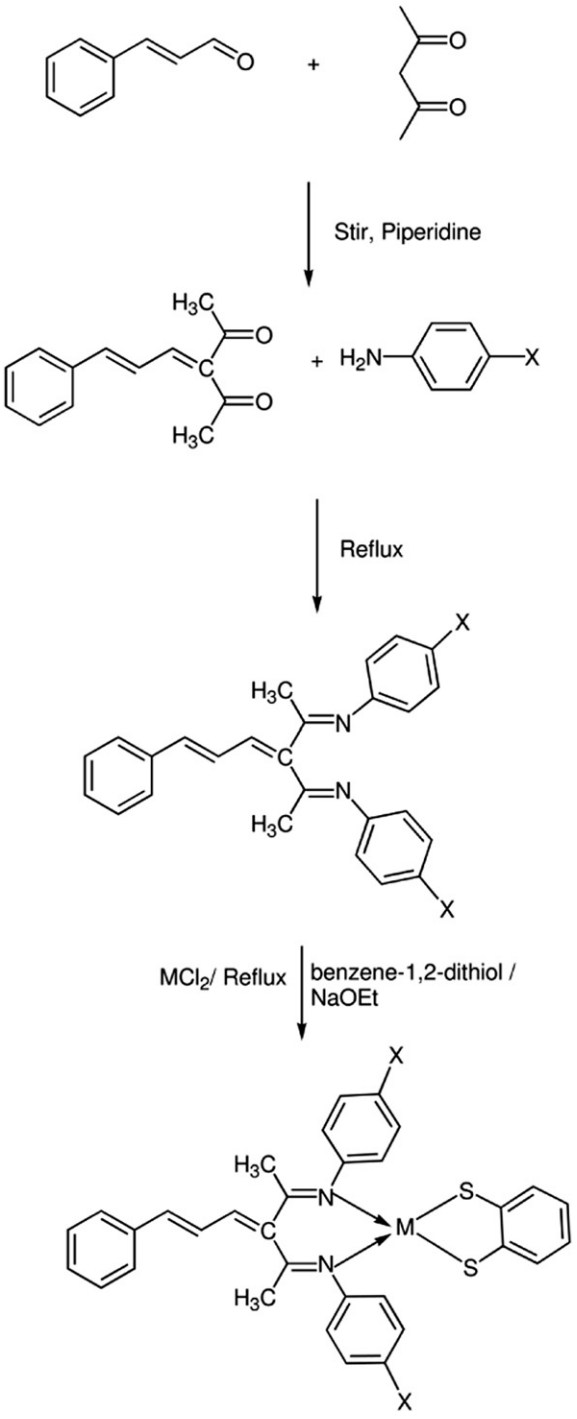

Scheme 1. Synthetic route for the preparation of complexes.

(MCF-7). The complexes were also investigated against *Mycobacterium tuberculosis* strain H37Rv. The minimal inhibitory concentration (MIC) of the complexes was determined.

4. Results and discussion

4.1. Chemistry

4.1.1. Infrared spectra

In IR spectra, the ν(C=N) band presented in the ligands was shifted to lower frequency by *ca.*30 cm^{-1} on complexation [26]. The free –OH group of the ligand L^3 vibrated at *ca.* 3435 cm^{-1} [26] did not show any significant shift on complex formation. The absence of ν(–SH) band, which appeared around 2550–2600 cm^{-1} as strong band, indicated the evidence of coordination of thiolate ligand through metal ion. Coordination of thiolate ligand with metal ion was also proven by the appearance of a ν(C–S) band in the region 1050–1150 cm^{-1} as strong vibration. It was further supported by the appearance of a new band in the region 380–410 cm^{-1} for all the complexes, assigned to the M–S band vibration and another new band observed in the region 434–452 cm^{-1} for all the complexes, attributed to the M–N vibration [27].

4.1.2. Electronic spectra and magnetic moments

The geometry of the metal complexes had been deduced from electronic spectra and magnetic moment data of the complexes. The free ligands exhibited two intense bands at 46256–41854 and 28965–27635 cm^{-1} which are due to $\pi \rightarrow \pi^*$ and $n \rightarrow \pi^*$ transitions respectively. In all metal complexes, these absorption bands were observed at 44345–40816 and 29876–35428 cm^{-1}. It indicates the coordination of the ligands with metal ions. The electronic spectra of Cu(II) complexes showed two broad, unusually high intensity (ε = 1800–3650 M^{-1} cm^{-1}) shoulder bands in the visible region, around 16949–17035 and 14684–14815 cm^{-1}, which are assigned to $^2B_{1g} \rightarrow {}^2A_{1g}$ and $^2B_{1g} \rightarrow {}^2E_g$ transitions respectively. The electronic spectral data suggest a square-planar geometry around the Cu(II) ion. The observed magnetic moment of the Cu(II) complexes (1.84–1.92 B.M) at room temperature indicates the non-coupled mononuclear complexes of magnetically diluted d^9 system with S = 1/2 spin-state square-planar structure. The monomeric nature of the complexes was further supported by the microanalytical and FAB mass spectral data. The electronic absorption spectra of the diamagnetic Zn(II) complexes showed bands at 38759–37453, 24213–24331 and 23866–23041 cm^{-1} which were assigned to intra-ligand charge transfer transitions [28].

4.1.3. NMR spectra of zinc complexes

The NMR spectra of ligands and their diamagnetic Zn(II) complexes were recorded in DMSO-d_6. In ^{1}H NMR, a set of mutiplets in the range of δ 6.8–7.8 ppm, observed for all the ligands and their Zn(II) complexes are assigned to aromatic region. The phenolic –OH proton for L^3 ligand and its zinc complexes was observed as a singlet *ca.* δ 11.8 and 11.4 ppm respectively. It is suggesting that phenolic –OH group is not taking part in the complexation. The absence of –SH proton in all the complexes in the region ~δ 7.8 ppm suggested the deprotonation of –SH group. This result indicates that the thiolate group involves in the coordination with metal ion upon complexation. ^{1}H NMR spectra of aliphatic methyl protons exhibited at δ 2.1–2.6 ppm for all the Schiff base ligands and their Zn(II) complexes. The peaks at δ 6.8–7.1 ppm were assigned to phenyl protons.

The ^{13}C NMR spectra of the ligands and their zinc complexes were recorded in DMSO-d_6. The aromatic carbon peaks were observed at δ 120.0–130.0 ppm. The ligands showed signal at δ 156.0–159.0 ppm indicating the presence of azomethine–carbon in the ligands. The downfield shift of this signal in the complexes (δ 162.0–165.0 ppm) indicated the coordination of azomethine nitrogen to metal. A new peak appeared in all the complexes in the region of δ 132–135 ppm indicating the presence of thiolate carbon atom. The solvent DMSO-d_6 carbon peak appeared at δ 39.7 ppm.

4.1.4. Mass spectra

The mass spectrum of L^3 ligand showed M + 1 peak at *m*/*z* 397 (15.6%) corresponding to $[C_{26}H_{24}N_2O_2]^+$ ion. Moreover, the spectrum exhibited the fragments at *m*/*z* 107, 77 and 66 corresponding to $[C_6H_5NO]^+$, $[C_6H_5]^+$ and $[C_5H_6]^+$ respectively. The mass spectrum of $[CuL^3(bdt)]$ showed peaks at *m*/*z* 598 and 599 with 19.8 and 15.7% abundances, respectively. The peak at *m*/*z* 598 may represent the molecular ion peak of the complex and the other peaks are isotopic species. The strongest peaks (base peak) at *m*/*z* 397 and 283 represent the stable species $C_{26}H_{24}N_2O_2$ and $C_{18}H_{10}N_4$ respectively. Also, the spectrum exhibited the fragments at *m*/*z* 107, 77 and 66 corresponding to $[C_6H_5NO]^+$, $[C_6H_5]^+$ and $[C_5H_6]^+$ respectively. The *m*/*z* of all the fragments of ligands and their complexes confirmed the stoichiometry of the complexes is being of the type [ML(bdt)]. It was further supported by the mass spectra of all the complexes. The observed peaks were in good agreement

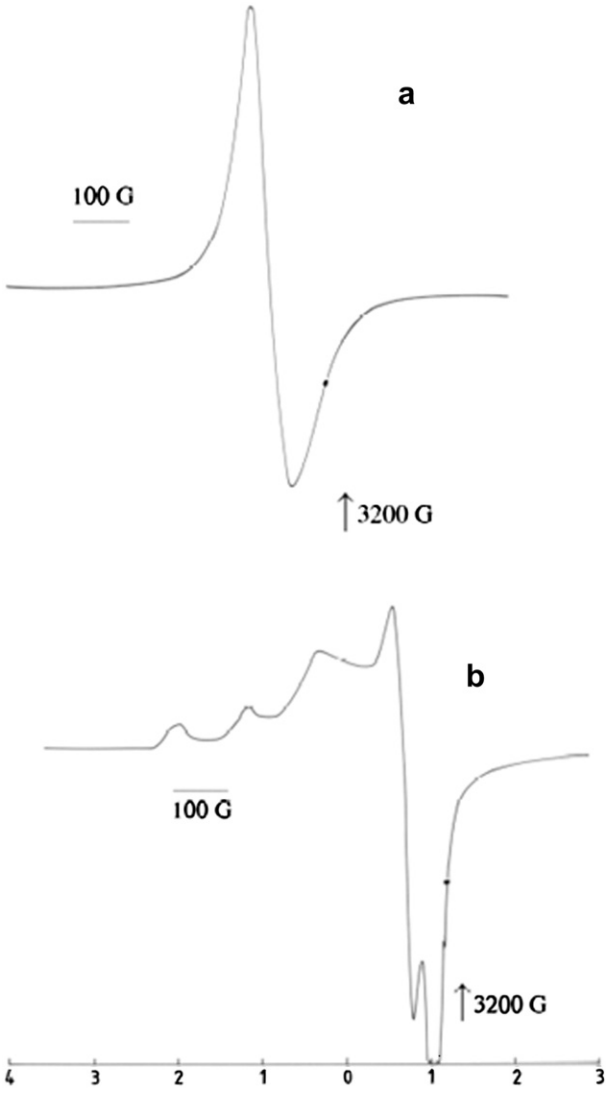

Fig. 1. EPR spectra of $[CuL^1(bdt)]$ at 300 K (a) and 77 K (b).

Table 1
The spin Hamiltonian parameters of Cu(II) complexes in DMSO at 300 K and 77 K.

Complexes	g-tensor			$A \times 10^{-4}$ (cm^{-1})			$g_{\|}/A_{\|}$	G
	$g_{\|}$	$g_{\perp}$	g_{iso}	$A_{\|}$	$A_{\perp}$	A_{iso}		
[CuL^1(bdt)]	2.18	2.07	2.15	125.2	18.5	63.9	182	4.12
[CuL^2(bdt)]	2.23	2.12	2.11	125.8	21.3	74.5	186	4.16
[CuL^3(bdt)]	2.26	2.09	2.16	120.6	23.7	68.3	194	4.20
[CuL^4(bdt)]	2.21	2.05	2.13	108.9	20.2	80.5	202	4.10

with their empirical formulae as indicated from microanalytical data. Thus, the mass spectral data reinforced the conclusion drawn from the analytical and conductance values.

4.1.5. EPR spectral study

The EPR spectra of all of the copper(II) complexes were recorded in DMSO at 300 and 77 K (Fig. 1). The spin Hamiltonian parameters calculated for the complexes are given in Table 1. The $g_{\|}$ values are greater than the corresponding $g_{\perp}$ values and therefore the unpaired electron occupies the $d_{x^2-y^2}$ molecular orbital [29]. All the spectra exhibited a typical four-line pattern. The spectral data were consistent with typical monomers but with distorted tetrahedral copper(II) geometry [30]. It is known that as the tetrahedral distortion increases, the $g_{\|}$ will increase with a decrease in $A_{\|}$ [31]. For blue copper proteins the $A_{\|}$ values are in the $15-90 \times 10^{-4}$ cm^{-1} region due to deviation from planarity, towards a suppressed tetrahedron. The observed $A_{\|}$ values ($\sim 110 \times 10^{-4}$ cm^{-1}) revealed the large deviation of the complexes from the regular square-planar geometry. The $A_{\|}$ values of these complexes are on the borderline between naturally occurring blue copper proteins and typical planar structures. Often the $g_{\|}/A_{\|}$ quotient is empirically treated as an index of tetrahedral distortion [30]. The $g_{\|}/A_{\|}$ values are expected to be in the 105–135 and 150–250 range respectively for square-planar and tetrahedral distorted copper(II) complexes. In the present case the $g_{\|}/A_{\|}$ values are between 182 and 202; it is assumed that they have geometry distorted from planarity towards tetrahedral. It is also reflected in the unusual gain in intensity in the visible spectra. According to Hathaway [32,33], the *G* values within the range 4.1–4.2 for all copper complexes indicate negligible exchange interaction of Cu–Cu in the complexes.

Based on the above analytical and spectral data, the structure of complexes is shown in Fig. 2.

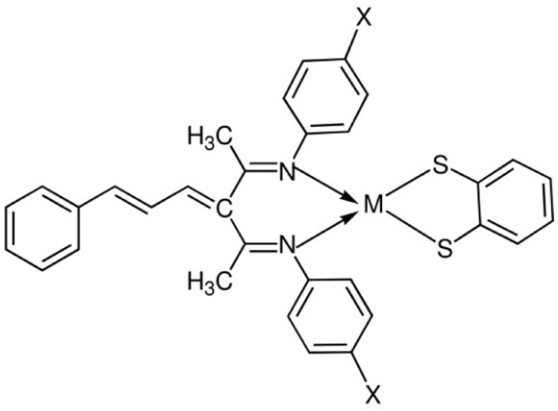

X	M	
$-NO_2$	Cu	[CuL^1(bdt)]
$-NO_2$	Zn	[ZnL^1(bdt)]
–H	Cu	[CuL^2(bdt)]
–H	Zn	[ZnL^2(bdt)]
–OH	Cu	[CuL^3(bdt)]
–OH	Zn	[ZnL^3(bdt)]
$-OCH_3$	Cu	[CuL^4(bdt)]
$-OCH_3$	Zn	[ZnL^4(bdt)]

Fig. 2. Structure of complexes.

4.2. Pharmacology

4.2.1. DNA binding studies

4.2.1.1. Electronic spectral studies. Electronic absorption spectra are initially employed to study the binding of complexes and DNA. Binding of complex to DNA through intercalation usually results in hypochromism and red shift (bathochromism), due to the intercalative mode involving a strong stacking interaction between aromatic chromophore and the base pairs of DNA. The extent of the hypochromism in the visible MLCT band is commonly consistent with the strength of intercalative interaction [34–36].

The electronic spectra of all the copper complexes exhibited a single d–d band around 610 nm as well as a more intense S (σ) → Cu(II) ligand to metal charge transfer (LMCT) band around 410 nm and 430 nm [37,38]. On the addition of calf thymus DNA a considerable decrease in absorptivity of the LMCT band was observed for all the complexes and the change in the absorbance for [CuL^1(bdt)] as a function of added DNA is shown in Fig. 3. There is a considerable decrease in the absorbance only upto R = 20 (R = [NP]/[Copper complex]).

The intercalative binding of colored drugs to DNA helix has been characterized by large changes in the absorbance (hypochromism) and appreciable shifts in wavelength (red shift) [39]. The observed hypochromism in the present case is very large compared to that observed for potential intercalators [40]. Since the present complexes do not contain any fused aromatic ring to facilitate intercalation, it is clear that the weak M–S bonds in the complex facilitate ligand displacement on adding DNA and that the interaction of DNA with metal(II) through sugar–phosphate oxygen, N7 of purines *etc.*, is stabilized. However, all the complexes do not undergo complete ligand displacement even if R value reaches 25. It appears that all the complexes bind to DNA through its axial position [38]. This leads to labilization of the complexes followed by displacement of thiolato ligands by DNA. Moreover, the planarity of the CuN_2S_2 chromophore of the complexes encourages its partial intercalation between the base pairs of DNA and stabilizes the complex against ligand displacement.

Also absorption spectral titrations of all the present complexes with ATP were carried out to understand their susceptibility towards ligand displacement. At the [ATP]:[complex] ratio of 1:1 for all the complexes complete displacement occurs suggesting the formation of a 1:1 Cu^{2+}:ATP complex obviously involving N(7) and

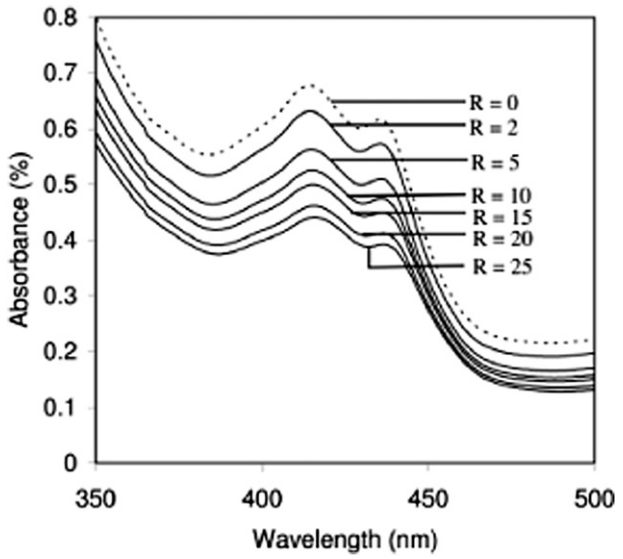

Fig. 3. Charge transfer spectrum of [CuL^1(bdt)] in the absence (—) and the presence (—) of increasing amount of CT DNA; R = [NP]/[complex].

phosphate oxygens of ATP [41]. So it is clear that similar donors present in DNA displace the thiolate ligands bound to metal.

In order to compare the binding strength of the complexes with CT DNA, the intrinsic binding constants K_b were obtained by monitoring the changes in absorbance for the complexes with increasing concentration of DNA. K_b was obtained from the ratio of slope to the intercept from the plots of [DNA]/($\varepsilon_a - \varepsilon_f$) *versus* [DNA]. The K_b values of copper and zinc complexes are shown in Table 2. The high K_b value for all complexes is due to the labialization of weak M–S bonds and flexible versatile ligands in complexes which greatly facilitate groove binding/stacking with the base pairs. The binding strength of the synthesized complexes with DNA is shown as in the following order: $-NO_2 > -OH > -OCH_3 > -H$.

4.2.1.2. Electrochemical behavior. The application of electrochemical methods to the study of metallointercalation and coordination of metal ions and chelates to DNA provides a useful complement to the previously used methods of investigation such as UV–Vis spectroscopy. As further exploring the binding of the present complexes with DNA, cyclic and differential pulse voltammetric studies were carried out both in the presence and absence of DNA.

Table 2
Charge transfer properties of interaction of synthesized complexes with CT DNA.

Sl. No	Complexes	λ_{max} (nm)		$\Delta\lambda$ (nm)	%H	M
		Free	Bound			
1	[CuL^1(bdt)]	413.0	416.0	3.0	19	2.4
		434.0	438.0	4.0	19	2.2
2	[CuL^2(bdt]	394.0	396.4	2.4	12	1.2
		420.4	423.2	2.8	13	1.1
3	[CuL^3(bdt)]	408.5	411.6	3.1	17	2.0
		428.3	430.7	2.7	16	2.0
4	[CuL^4(bdt)]	400.7	403.3	2.6	12	1.9
		425.6	427.8	2.2	12	1.9
5	[ZnL^1(bdt)]	417.1	419.5	2.4	10	1.8
		429.6	431.8	2.2	09	1.8
6	[ZnL^2(bdt)]	403.3	404.8	1.5	05	1.0
		419.7	420.9	1.2	07	0.9
7	[ZnL^3(bdt)]	413.4	415.0	2.4	11	1.7
		425.6	426.3	0.7	12	1.0
8	[ZnL^4(bdt)]	409.7	410.8	1.1	09	1.0
		421.8	423.9	2.1	09	1.3

The cyclic voltammogram of the complexes in buffer (Table 3) reveals a non-Nernstian behavior of the Cu(II)/Cu(I) couple, as may be judged from the limiting peak potential separation (ΔEp°, ΔEp value extrapolated to zero scan rate) of 62–78 mV (59 mV for a one-electron diffusion controlled reversible process). Redox behavior of [CuL^1(bdt)] in DMF *versus* Ag/AgCl with TBAP as supporting electrolyte at different scan rate is shown in Fig. 4. Linearity of the i_{pc} *versus* square root of scan rate plot (passing through origin) and the values of i_{pa}/i_{pc} (≈ 1) suggest that the redox tends to become fairly reversible. The redox potentials of the present complexes follow the trends [CuL^4(bdt)] > [CuL^3(bdt)] > [CuL^2(bdt)] > [CuL^1(bdt)] illustrating the ability of chelate rings to stabilize the Cu(I) state. The later are expected to illustrate the nuclease activity of copper complexes, as their Cu(II) and Cu(I) forms are involved in the proposed cleavage mechanism (Scheme 2).

A typical CV behavior of synthesized complexes in the presence of excess DNA is shown in Fig. 5. A large decrease in peak currents of almost all the complexes on adding DNA is consistent with the displacement of the thio ligand in the complexes, revealed by spectral results. The shift in $E_{1/2}$ for complexes on binding to Cu^{2+}–DNA suggests that both Cu(II) and Cu(I) forms bind to DNA but to different extents. Analogous to the treatment of the association of small molecules with micelles [42] and DNA [43], the ratio of the equilibrium constants, K_{2+}/K_+ for the binding of the Cu(II) and Cu(I) forms of complexes to DNA can be estimated from the net shift in $E_{1/2}$, assuming reversible electron transfer. For a Nernstian electron transfer in a system in which both the oxidized and reduced forms associate with a third species such as DNA in solution, Scheme 2 can be applied. Here CuL^{n+}–DNA represents the CuL^{n+} complex bound to Cu^{2+}–DNA. Thus for the one-electron process,

$$E_b^{\circ\prime} - E_f^{\circ\prime} = 0.059\log(K_+/K_{2+})$$

where $E_f^{\circ\prime}$ and $E_b^{\circ\prime}$ are the formal potentials of the, Cu(II)/Cu(I) couple in the free and bound forms, respectively. Thus from the shift in $E_{1/2}$ values, K_{2+}/K_+ ratios were calculated.

For all the synthesized complexes K_{2+} was higher than K_+. This suggests that B-DNA with small C-DNA character tends to stabilize the Cu(II) over the Cu(I) state of the complex obviously by electrostatic interaction. The DNA strand which may be considered as a local 'solvent' environment as far as bound metal complex is concerned differs from the bulk medium in dielectric constant and charge distribution and so has a substantial effect on the electron transfer thermodynamics [44]. Further, as DNA has the hydrophilic coat/hydrophobic core structure [45], the interplay between electrostatic and hydrophobic (intercalative) interactions can be important in the overall binding of the charged species possessing a planar aromatic moiety [46].

In addition to changes in the formal potential, the voltammetric current decreased upon the addition of Cu^{2+}–DNA as shown in Table 3. The decrease in current in CV experiments may be attributed to the diffusion of copper complexes bound to the large, slowly diffusing DNA molecule. The change in current upon Cu^{2+}–DNA addition can be explained in terms of the diffusion of an equilibrium mixture of free and Cu^{2+}–DNA-bound metal complex to the electrode surface. The slope of the $i_{pc} - \nu^{1/2}$ plot decreased with increase in the ratio R (=[NP]/[Cu complex]), indicating a reduction in the apparent diffusion coefficient of copper complexes as [NP] is increased. This decrease in the diffusion coefficient value with increase in R reveals the quantitative binding of the complex to DNA. The ratio of anodic to cathodic peak current, i_{pa}/i_{pc}, was less than unity under all experimental conditions, indicating that the Cu (II) complex species is stable on the time scale of the CV measurement. It was further supported by the differential pulse voltammogram experiment which is shown in Fig. 6.

Table 3
Electrochemical parameters of interaction of copper complexes with CT DNA.

Sl. No	Complexes	蜘Ep (V)		$E_{1/2}$ (V)		Decrease of i_{pc} (%)	i_{pa}/i_{pc}		K_+/K_{2+}
		Free	Bound	Free	Bound		Free	Bound	
1	[CuL^1(bdt)]	0.727	0.597	0.493	0.558	41	0.59	0.77	0.07
2	[CuL^2(bdt)]	0.645	0.432	0.470	0.380	34	0.79	0.54	0.18
3	[CuL^3(bdt)]	0.567	0.322	0.492	0.439	27	0.72	0.61	0.34
4	[CuL^4(bdt)]	0.529	0.553	0.383	0.568	19	0.76	0.61	0.52

These results demonstrate that rather straightforward electrochemical methods can be employed to characterize the intercalative interaction between a metal complexes or electro active species and DNA. The electrochemical oxidation and reduction of selected bound species on DNA can also be carried out and favorable circumstances may allow strand scission in the DNA.

The electrochemical behavior of all the zinc complexes in the absence of DNA showed only cathodic potential corresponding to Zn(II/0). The cathodic peak appeared in the positive potential of 0.812–0.924 V range corresponding to the two electron reduction of Zn(II) complexes. Addition of CT DNA to the zinc complexes solution resulted in a shift of cathodic peak potentials to more negative values and a decrease of the cathodic currents. The shift of the cathodic potential of the complexes in the presence of DNA to more negative values indicates a binding interaction between the complexes and DNA that makes the complexes less readily reducible. The drop of the voltammetric currents in the presence of CT DNA can be attributed to diffusion of metal complexes bound to higher and slowly diffusing DNA molecule. The decreased extents of the peak currents observed for the complexes upon addition of DNA may indicate copper complexes possess more DNA-binding affinity than zinc complexes. Typical voltammetric data of zinc complexes at different DNA concentrations are summarized in Table 4.

Differential pulse voltammogram of the Zn(II) complexes observed a positive potential shift along with significant decreasing of current intensity during the addition of increasing amounts of DNA. It indicates that zinc ions stabilize the duplex (GC pairs) by intercalating way. Hence, the complexes of the electroactive species (Zn(II)) with DNA, the electrochemical reduction reaction can be divided into two steps:

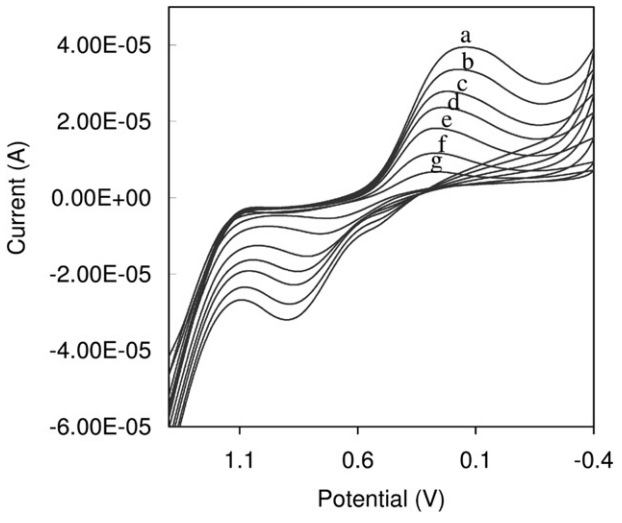

Fig. 4. Redox behavior of [CuL^1(bdt)] in DMF *versus* Ag/AgCl with TBAP as supporting electrolyte at scan rate (a) 150, (b) 125, (c) 100, (d) 75, (e) 50, (f) 25, and (g) 10 mV s^{-1}.

$$Zn^{2+} - DNA \rightleftharpoons Zn^{2+} + DNA$$

$$Zn^{2+} - 2e^- \rightleftharpoons Zn^0$$

The dissociation constant (K_d) of the Zn(II)–DNA complex was obtained using the following equation:

$$i_p^2 = \frac{K_d}{[DNA]}\left(i_p^2 o - i_p^2\right) \rightleftharpoons i_p^2 o - [DNA]$$

where K_d is dissociation constant of the complex Zn(II)–DNA, $i_p^2 o$ and i_p^2 are reduction current of Zn(II) in the absence and presence of DNA respectively. The low dissociation constant values (Table 4) of Zn(II) ions were indispensable for structural stability of complexes Zn(II)–DNA which participate in the replication, degradation and translation of genetic material of all species.

4.2.1.3. Viscosity measurements. Under appropriate conditions intercalation causes a significant increase in the viscosity of DNA solutions due to the increase in the separation of base pairs at intercalation sites and hence an increase in overall DNA contours length. By contrast, ligands that bind exclusively in the DNA grooves (*e.g.* netropsin, distamycin), under the same conditions, typically cause less pronounced changes (positive or negative) or no changes in DNA solution viscosity [44]. As a means for further exploring the binding of the copper complexes, viscosity measurements were carried out on DNA pretreated with copper(II) chloride by varying the concentration of the added complexes. The values of relative specific viscosity (η/η^o), where η^o is the specific viscosity contribution of DNA in the absence of complex, were plotted against 1/R (=[complex]/[NP]) (Fig. 7a and b). The synthesized complexes slightly decreased the specific viscosity of DNA possibly due to a number of factors including a change in conformation, flexibility or solvation of DNA molecules. However, in view of the tendency of DNA towards particulate formation, it is most likely that extensive aggregation of DNA on binding to the complexes [47] would sharply reduce the number of independently moving DNA molecules in solution and hence the viscous drag that comes from molecules diffusing into each other. Thus, a similar decrease in η/η^o for other complexes has been ascribed to DNA aggregation [47]. In contrast to all the complexes exhibit two distinct modes of binding; the relative specific viscosity increases slowly up to 1/R = 0.25 and then steadily but the extent of increase is lesser than that for the known intercalator, ethidium bromide

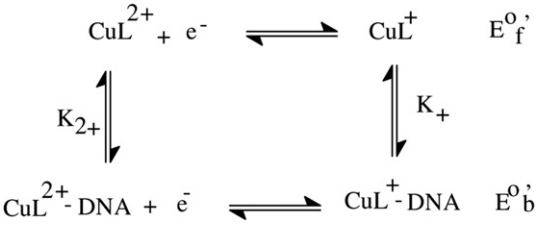

Scheme 2. Redox behavior of copper complex in the presence of DNA.

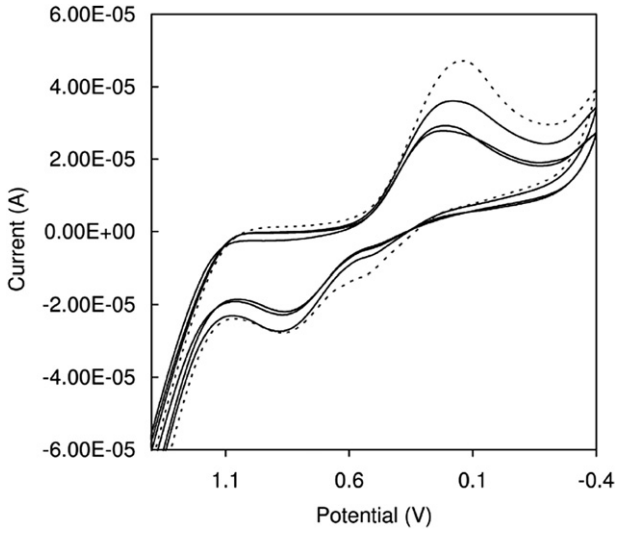

Fig. 5. Redox behavior of [CuL^1(bdt)] both in the absence (—) and the presence (—) of different concentration of DNA using cyclic voltammogram. Supporting electrolyte, 50 mM NaCl, 5 mM Tris–HCl, pH = 7.1. Scan rate 100 mV s^{-1}.

(EB) [48] illustrating the partial stacking interaction of complexes with DNA as discussed above. Spectral and electrochemical evidences also support such an intercalative mode of interaction.

4.2.2. DNA cleavage studies

4.2.2.1. Chemical nuclease activity. Gel electrophoresis experiments using pUC19 circular plasmid DNA were performed with the ligands and their complexes in the presence and absence of H_2O_2 as an oxidant. At micro-molar concentrations, for 2 h incubation periods, the ligands exhibited no significant cleavage activity in the absence or presence of oxidant (H_2O_2). The nuclease activity was greatly enhanced by the incorporation of metal ion in the respective ligands. The nuclease activity of the complexes was also investigated in the presence of a free radical scavenger, dimethylsulfoxide (DMSO) and singlet oxygen quencher, azide ion (NaN_3). From Fig. 8a and b, it is evident that the complexes cleave DNA more efficiently in the presence of an oxidant. This may be attributed to the formation of hydroxyl free radicals. The production of a hydroxyl radical due to

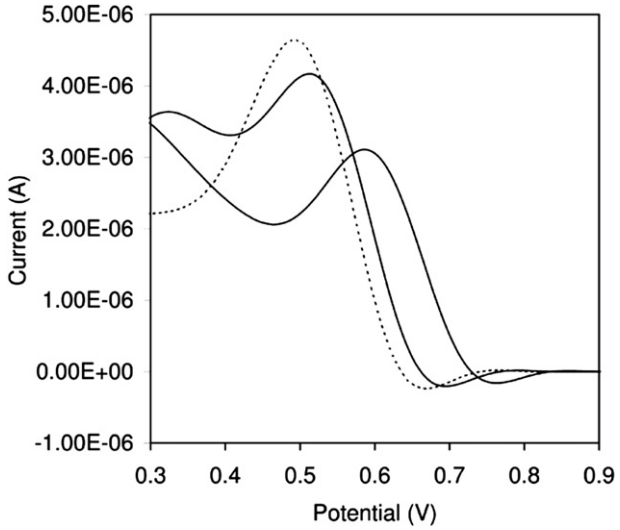

Fig. 6. Redox behavior of [CuL^1(bdt)] both in the absence (—) and the presence (—) of different concentration of DNA using differential pulse voltammogram. Supporting electrolyte, 50 mM NaCl, 5 mM Tris–HCl, pH = 7.1. Scan rate 100 mV s^{-1}.

Table 4
Electrochemical parameters of interaction of zinc complexes with CT DNA.

Sl. No	Complexes	Ep (V)		i_{pc} (μA)		$K_d \times 10^{-10}$ (mol L^{-1})
		Free	Bound	Free	Bound	
1	[ZnL^1(dppz)]Cl$_2$	0.924	0.932	0.63	0.40	3.2
2	[ZnL^2(dppz)]Cl$_2$	0.884	0.893	0.59	0.41	2.3
3	[ZnL^3(dppz)]Cl$_2$	0.841	0.848	0.60	0.52	2.1
4	[ZnL^4(dppz)]Cl$_2$	0.812	0.823	0.47	0.38	1.6

the reaction between the metal complex and oxidant may be explained as follows:

$$Cu(II)L + e^- \rightarrow Cu(I)L$$

$$Cu(I)L + O_2 \rightarrow Cu(II)L + O_2^-$$

$$2O_2^- + 2H^+ \rightarrow H_2O_2 + O_2$$

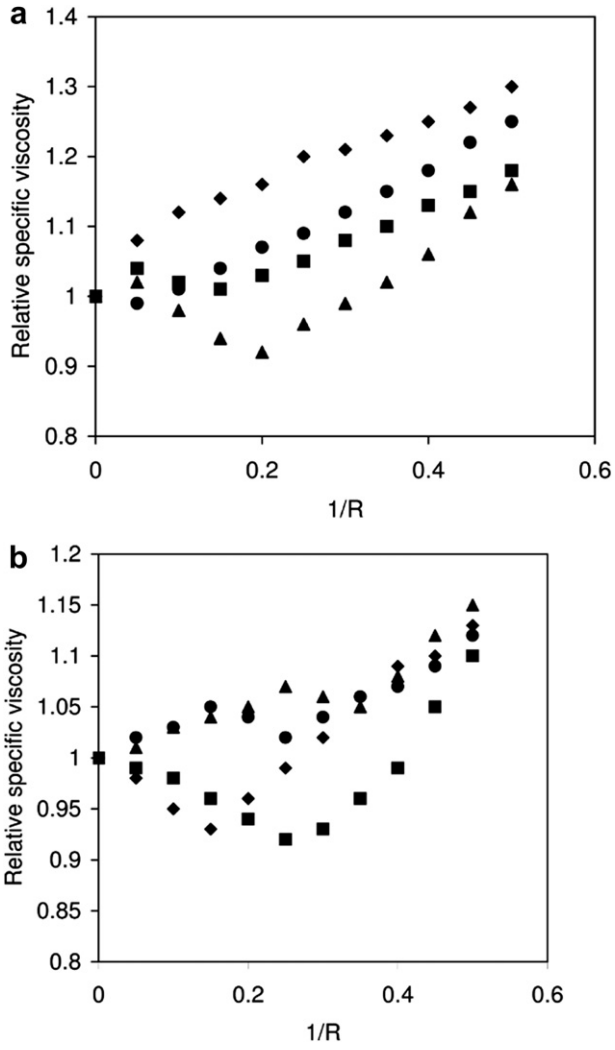

Fig. 7. (a). Ratio of the specific viscosity of DNA in the presence of copper complex to that of free CT DNA vs. 1/R (=[Copper complex]/[NP]) in the presence of [CuL^1(bdt)] (◆), [CuL^2(bdt)] (▲), [CuL^3(bdt)] (●) and [CuL^4(bdt)] (■). (b). Ratio of the specific viscosity of DNA in the presence of zinc complex to that of free CT DNA vs. 1/R (=[Zinc complex]/[NP]) in the presence of [ZnL^1(bdt)] (▲), [ZnL^2(bdt)] (◆), [ZnL^3(bdt)] (●) and [ZnL^4(bdt)] (■).

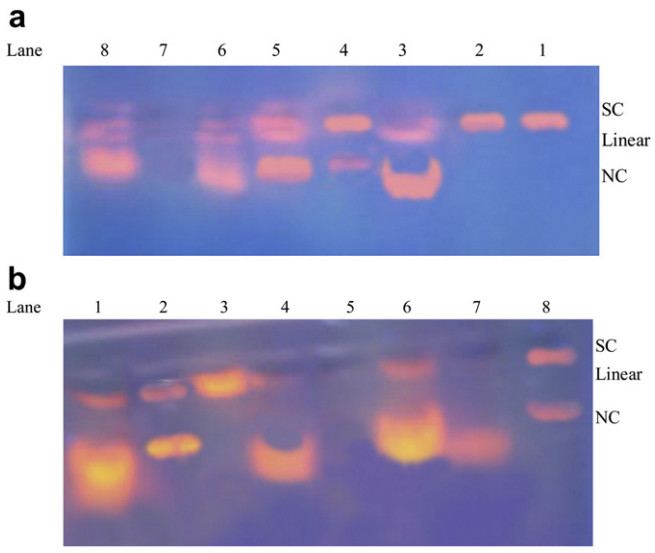

Fig. 8. (a). Gel electrophoresis diagram showing the cleavage of SC pUC19 DNA (0.2 μg) by the synthesized complexes (50 μM) in the presence of MPA (5 mM): lane 1, DNA control; lane 2, DNA + L^1 (50 μM); lane 3, DNA + [CuL^1(bdt)] + H_2O_2; lane 4, DNA + [CuL^1(bdt)] + DMSO (4 μL) + H_2O_2; lane 5, DNA + [CuL^1(bdt)] + distamycin (50 μM) + H_2O_2; lane 6, DNA + [CuL^1(bdt)] + SOD (1U) + H_2O_2; lane 7, DNA + L^2; lane 8, DNA + [CuL^2(bdt)] + H_2O_2. (b). Gel electrophoresis diagram showing the cleavage of SC pUC19 DNA (0.2 μg) by the synthesized complexes (50 μM) in the presence of MPA (5 mM): lane 1, DNA + [CuL^2(bdt)] + distamycin (50 μM) + H_2O_2; lane 2, DNA + [CuL^2(bdt)] + DMSO (4 μL) + H_2O_2; lane 3, DNA + L^3; lane 4, DNA + [CuL^3(bdt)] + H_2O_2; lane 5, DNA + L^4; lane 6, DNA + [CuL^4(bdt)] + H_2O_2; lane 7, DNA + [CuL^4(bdt)] + DMSO (4 μL) + H_2O_2; lane 8, DNA + [CuL^4(bdt)] + NaN_3.

$$Cu(I)L + H_2O_2 \rightarrow Cu(II)L + OH^- + OH^\bullet$$

$$O_2^- + H_2O_2 \rightarrow O_2 + OH^- + OH^\bullet$$

These OH free radicals participate in the oxidation of the deoxyribose moiety, followed by hydrolytic cleavage of the sugar phosphate backbone [49]. The more pronounced nuclease activity of these adducts in the presence of oxidant as compared to the parent copper complexes may be due to the increased production of hydroxyl radicals. Even in the absence of oxidant, the mixed ligand complexes exhibit significant DNA cleavage activity when compared to the parent complexes. This may be due to the ability of the mixed ligand complexes to associate with DNA, facilitated by hydrophobic interaction leading to fair nucleolytic cleavage. It is clear that the order of cleavage activity in the presence of oxidant (H_2O_2) follows the order [CuL^1(bdt)] > [CuL^3(bdt)] > [CuL^4(bdt)] > [CuL^2(bdt)]. To determine the groove selectivity of the complexes, control experiments were performed using minor groove binder distamycin. The addition of distamycin did not inhibit the cleavage for the complexes. This result suggests major groove binding for the complexes.

The nuclease activity of the complexes had also been investigated in the presence of a free radical scavenger (dimethylsulfoxide) and a singlet oxygen quencher (azide ions). To this end, standard scavengers of reactive oxygen intermediates were included in the electrophoresis process (Fig. 8a and b). Azide inhibited to some extent, indicating the involvement of singlet oxygen in the cleavage activity. The hydroxyl radical scavenger, dimethylsulfoxide diminished the nuclease activity of the compound, which is indicative of the involvement of the hydroxyl radical in the cleavage process. Nuclease activity of the complexes was not completely diminished either in the presence of free radical scavenger or in the presence of singlet oxygen quencher. It means that some DNA was cleaved by other than an oxidative mechanism, possibly by a discernable hydrolytic path.

4.2.2.2. Hydrolytic cleavage and ligation of the DNA linearized by zinc(II) complexes. Although the cleavage reaction through zinc complexes does not require additional external agents, we carefully investigated the possibility that diffusible OH radical, singlet oxygen ($^1O_2$) or superoxide anion radical were involved in this reaction. The cleavage efficiency does not change in the presence of DMSO as potential OH radical scavengers, NaN_3 as potential $^1O_2$ inhibitors, or SOD as a superoxide anion radical inhibitor [50–52]. In conclusion, the results presented here rule out the involvement of any oxidation inhibitors in the strand cleavage, and this reaction most probably occurs through a hydrolytic mechanism. Further experiments support this assumption. It is well known that in DNA hydrolytic cleavage 3′-OH and 5′-OPO_3 (5′-OH and 3′-OPO_3) fragments remain intact and that these fragments can be enzymatically ligated and end-labeled. Fig. 9a and b shows that the linear DNA fragments cleaved by zinc complex can be relegated by T4 ligase just like the linear DNA mediated by EcoR1. Hence, this result implied that the process of DNA cleavage by the complex occurs *via* a hydrolytic path.

4.2.2.3. Photonuclease activity. Photo-induced DNA cleavage experiments were carried out in UV and visible light using the ligands and their copper complexes (50 and 100 μM) and SC pUC19 DNA (0.2 μg, 33.3 μM) in the presence and absence of various inhibitors.

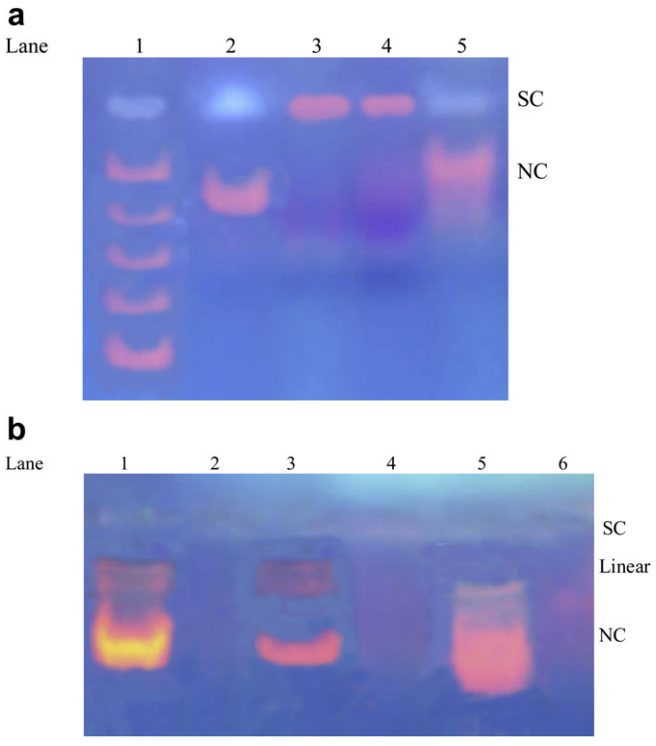

Fig. 9. (a). Gel electrophoresis diagram for ligation of SC pUC19 DNA linearized by zinc complexes: lane 1, DNA markers; lane 2, DNA + [ZnL^1(bdt)]; lane 3, DNA + [ZnL^1(bdt)] + T4 DNA ligase; lane 4, DNA + [ZnL^1(bdt)] + EcoR1; lane 5, DNA + [ZnL^1(bdt)] + EcoR1 + T4 DNA ligase. (b). Gel electrophoresis diagram for ligation of SC pUC19 DNA linearized by zinc complexes: lane 1, DNA + [ZnL^2(bdt)]; lane 2, DNA + [ZnL^2(bdt)] + T4 DNA ligase; lane 3, DNA + [ZnL^3(bdt)]; lane 4, DNA + [ZnL^3(bdt)] + T4 DNA ligase; lane 5, DNA + [ZnL^4(bdt)]; lane 6, DNA + [ZnL^4(bdt)] + T4 DNA ligase.

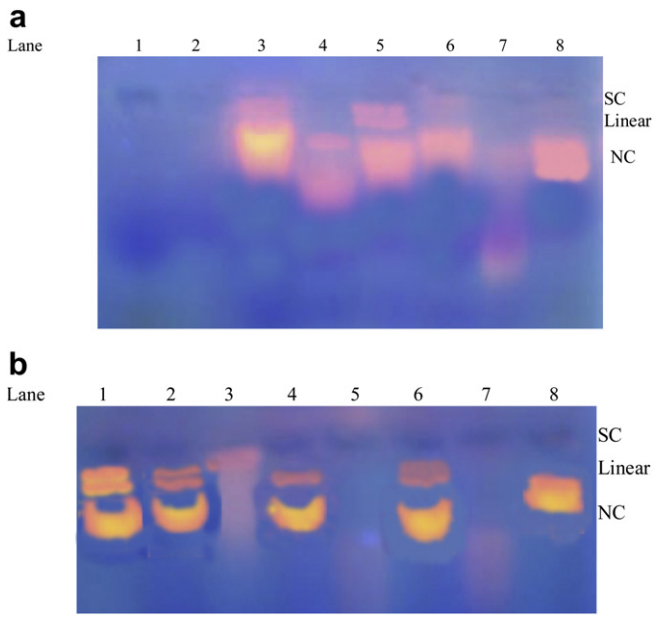

Fig. 10. (a). Gel electrophoresis diagram showing the photocleavage of pUC19 DNA by the synthesized complexes in DMF–Tris buffer medium and in the presence of various reagents on irradiation with UV light at 360 nm: lane 1, DNA control (60 min); lane 2, DNA + L^1 (60 min); lane 3, DNA + [CuL^1(bdt)] + D_2O (60 min); lane 4, DNA + [CuL^1(bdt)] (60 min); lane 5, DNA + [CuL^1(bdt)] + DMSO (60 min); lane 6, DNA + [CuL^1(bdt)] + SOD (60 min); lane 7, DNA + [CuL^1(bdt)] + NaN_3 (60 min); lane 8, DNA + [CuL^2(bdt)] (60 min). (b). Gel electrophoresis diagram showing the photocleavage of pUC19 DNA by the synthesized complexes in DMF–Tris buffer medium and in the presence of various reagents on irradiation with UV light at 360 nm: lane 1, DNA + [CuL^2(bdt)] + D_2O (60 min); lane 2, DNA + [CuL^2(bdt)] + DMSO (60 min); lane 3, DNA + [CuL^2(bdt)] + NaN_3 (60 min); lane 4, DNA + [CuL^2(bdt)] + SOD (60 min); lane 5, DNA + L^3 (60 min); lane 6, DNA + [CuL^3(bdt)] (60 min); lane 7, DNA + L^4 (60 min); lane 8, DNA + [CuL^4(bdt)] (60 min).

The DNA cleavage of ligand alone was inactive. The result indicated the importance of the metal in the complexes for observing the photo-induced DNA cleavage activity. All the complexes cleaved the pUC19 DNA from its SC to NC form even in the absence of inhibitors on irradiation with UV light at 360 nm. In the presence of singlet oxygen quencher like sodium azide inhibited the cleavage. An enhancement of photocleavage of DNA was observed in D_2O solvent in which $^1O_2$ had longer life time [53]. Hydroxyl radical scavenger DMSO or KI did not show any significant inhibition in the DNA cleavage activity. The results are indicative of the presence of a type-II in which the photo-excited complexes activate molecular oxygen from its stable triplet to the cytotoxic singlet state. Moreover, it suggests the formation of singlet oxygen as the respective species in a type-II process in the metal assisted photo-excitation process involving ligand $n-\pi^*$ and $\pi-\pi^*$ transitions (Fig. 10a and b).

Table 6
Effect of Cu(II) and Zn(II) complexes treatment on the survival of tumor-bearing mice.

Treatment	MST	Increase in life span
Tumor control	14.56 ± 0.56	–
5-FU	34.83 ± 0.87*	140.21
[CuL^1(bdt)]	30.17 ± 0.60*	108.06
[CuL^2(bdt)]	32 ± 0.58*	120.69
[CuL^3(bdt)]	30.83 ± 0.75*	112.62
[CuL^4(bdt)]	30 ± 0.58*	106.89
[ZnL^1(bdt)]	32.17 ± 0.95*	121.86
[ZnL^2(bdt)]	29.17 ± 0.60*	101.17
[ZnL^3(bdt)]	29.83 ± 0.79*	105.72
[ZnL^4(bdt)]	29.3 ± 1.20*	102.07

N = 6; d of drug treatment = 9, *$P < 0.01$ *versus* tumor control. Data were analyzed by one-way ANOVA followed by Dunnett's test.

4.2.3. Antitumor activity

4.2.3.1. Effect of complexes on hematological parameters. Hematological parameters of tumor-bearing mice on day 14 showed significant changes when compared with the normal mice (Table 5). The total white blood cell (WBC) count, proteins and packed cell volume (PCV) were found to increase with a reduction in the hemoglobin content of red blood cell (RBC). The differential count of WBC showed that the percentage of neutrophils increased ($P < 0.001$) while that of lymphocytes decreased ($P < 0.001$). At the same time interval, complexes (100 mg/kg/day, p.o.) treatment could change these altered parameters to near normal. The reliable criteria for judging the value of any anti-cancer drug are prolongation of lifespan and decrease of WBC from blood [54,55]. The results of the present study showed an antitumor effect of complexes against EAC in Swiss albino mice.

The analysis of the hematological parameters showed minimum toxic effect in mice treated with complexes. After 14 days of transplantation, complexes were able to reverse the changes in the hematological parameters consequent to tumor inoculation. The present study revealed that the complexes were cytotoxic towards EAC.

4.2.3.2. Effect of Cu(II) and Zn(II) complexes on survival time. The effect of complexes on the survival of tumor-bearing mice is shown

Table 5
Effect of Cu(II) and Zn(II) complexes on hematological parameters of EAC tumor-bearing mice.

Design of treatment	Hb (gm %)	RBC 10^6 Cells/CU.MM	WBC 10^3 Cells/CU.MM	Total protein mg%	PCV (%)	Differential count (%)		
						Lymphocytes	Neutrophils	Monocytes
Normal	12.92 ± 0.15	4.9 ± 0.12	6.78 ± 0.14	5.73 ± 0.26	16.86 ± 0.55	66.4 ± 1.36	32.6 ± 1.6	1 ± 0.45
Tumor control	5.78 ± 0.4[a]	2.46 ± 0.14[a]	18.74 ± 0.47[a]	12.23 ± 0.34[a]	25.98 ± 0.56[a]	26.2 ± 1.16[a]	72.8 ± 1.07[a]	1 ± 0.45
[CuL^1(bdt)]	12.48 ± 0.21[d]	4.26 ± 0.19[d]	15.54 ± 0.3[a,d]	7.44 ± 0.17[b,d]	17.02 ± 0.26[d]	64.2 ± 0.86[d]	35.2 ± 1.24[d]	0.6 ± 0.4
[CuL^2(bdt)]	12.38 ± 0.13[d]	3.44 ± 0.15[a,e]	14.96 ± 0.54[a,d]	7.62 ± 0.27[a,d]	16.98 ± 0.51[d]	68 ± 1.0[d]	31.6 ± 1.03[d]	0.4 ± 0.24
[CuL^3(bdt)]	11.04 ± 0.16[a,d]	3.94 ± 0.13[b,d]	12.16 ± 0.63[a,d]	8.56 ± 0.17[a,d]	17.1 ± 0.45[d]	63.2 ± 1.28[d]	36.2 ± 1.46[d]	0.6 ± 0.4
[CuL^4(bdt)]	13 ± 0.14[d]	4.84 ± 0.15[d]	11.4 ± 0.42[a,d]	7.96 ± 0.41[a,d]	19.98 ± 0.54[b,d]	61.4 ± 1.21[d]	38 ± 1.23[d]	0.6 ± 0.24
[ZnL^1(bdt)]	12.48 ± 0.29[d]	4.6 ± 0.21[d]	11.86 ± 0.32[a,d]	7.44 ± 0.24[b,d]	18.96 ± 0.43[d]	67.2 ± 1.93[d]	32.4 ± 2.11[d]	0.4 ± 0.4
[ZnL^2(bdt)]	11.1 ± 0.43[a,d]	4.2 ± 0.12[d]	12.54 ± 0.36[a,d]	8.14 ± 0.14[a,d]	17.2 ± 0.45[d]	65.6 ± 1.72[d]	33.8 ± 1.83[d]	0.6 ± 0.4
[ZnL^3(bdt)]	11.78 ± 0.27[d]	4.04 ± 0.21[c,d]	11.78 ± 0.32[a,d]	6.76 ± 0.23[d]	18.94 ± 0.71[d]	64.8 ± 1.28[d]	34.6 ± 1.63[d]	0.6 ± 0.4
[ZnL^4(bdt)]	12.28 ± 0.23[d]	3.92 ± 0.11[b,d]	11.04 ± 0.72[a,d]	7.06 ± 0.24[c,d]	18.04 ± 0.47[d]	64.6 ± 1.36[d]	35 ± 1.14[d]	0.4 ± 0.24

[a] $P < 0.001$.
[b] $P < 0.01$.
[c] $P < 0.05$ *versus* Normal.
[d] $P < 0.001$.
[e] $P < 0.01$ *versus* Tumor control. Data were analyzed by using one-way ANOVA followed by Tukey–Kramer multiple comparison test.

Table 7
In vitro cytotoxic activity of Cu(II) and Zn(II) complexes in EAC cell line.

Treatment compounds	IC_{50} (μg/mL)
[CuL^1(bdt)]	114.47
[CuL^2(bdt)]	190.55
[CuL^3(bdt)]	183.38
[CuL^4(bdt)]	108.18
[ZnL^1(bdt)]	170.59
[ZnL^2(bdt)]	182.35
[ZnL^3(bdt)]	175.40
[ZnL^4(bdt)]	186.56

Average of 3 determinations, 3 replicates IC_{50}, Drug concentration inhibiting 50% cellular growth following 3 h of drug exposure.

in Table 6. The MST of the treated groups was compared with those of control groups by the following calculation:

$$\text{Increase in life span} = \frac{T - C}{C} \times 100$$

where T = number of days treated animals survived and C = number of days control animals survived.

The basic criteria for any anti-cancer drug should prolong the life span of the tumor bearing animals. The effect of [CuL^2(bdt)] and [ZnL^1(bdt)] complexes on the survival of tumor-bearing mice showed at dose of 100 mg/mL a life span values 120.69 and 121.86% respectively. These complexes were judged to be significant anti-tumor activity against tumor-bearing mice. The other complexes were also showed significant increase in the life span of the tumor-bearing mice which were almost comparable with that of 5-FU. These results clearly demonstrated the antitumor effect of complexes against EAC.

4.2.3.3. Effect of Cu(II) and Zn(II) complexes on cytotoxicity in vitro. The *in vitro* cytotoxicity studies were performed by trypan blue dye exclusion method. The IC_{50} values of all the synthesized complexes were given in Table 7. Among the all of the complexes tested, [CuL^4(bdt)] and [CuL^1(bdt)] have lowest IC_{50} values of 108.18 and 114.47 μg/mL when compared with other complexes. From the result, it is inferred that [CuL^4(bdt)] and [CuL^1(bdt)] complexes have higher cytotoxicity and anti-cancer effects on cancer cell line than other complexes.

4.2.3.4. Effect of Cu(II) and Zn(II) complexes on human cancer cell lines by MTT assay. In vitro anti-cancer activity was assessed by MTT assay against human cervical cancer cell lines (HeLa), Human laryngeal epithelial cancer (Hep2), Human liver cancer (HepG2) and Human breast cancer (MCF-7). IC_{50} values of the complexes were displayed in Table 8. Cisplatin was used as standard. When the cells were treated for 72 h with various concentrations of complexes and cisplatin (0.1–100 μg/mL), relative cell survival progressively decreased in a dose-dependent manner. The IC_{50} of the synthesized complexes were determined for all cell lines. Among the complexes, [CuL^3(bdt)] showed low IC_{50} against HeLa and MCF-7 cell lines. However, all the complexes showed higher IC_{50} when compared to the standard cisplatin.

Table 8
In vitro cytotoxic effect of Cu(II) and Zn(II) complexes against human cancer cell lines.

Compounds	IC_{50} (μg/mL)			
	HeLa	Hep2	HepG2	MCF-7
[CuL^1(bdt)]	17	33	2	7
[CuL^2(bdt)]	34	52	14	18
[CuL^3(bdt)]	31	58	9	6
[CuL^4(bdt)]	14	26	8	3
[ZnL^1(bdt)]	36	54	16	14
[ZnL^2(bdt)]	30	34	24	21
[ZnL^3(bdt)]	42	46	22	24
[ZnL^4(bdt)]	44	52	26	31
Cisplatin	0.53	0.25	0.65	0.72

Average of 3 determinations, 3 replicates IC_{50}, Drug concentration inhibiting 50% cellular growth following 72 h of drug exposure.

Table 9
Minimum inhibitory concentration of complexes against *Mycobacterium tuberculosis*.

Complex	MIC (μg/mL)
[CuL^1(bdt)]	2.9
[CuL^2(bdt)]	>100
[CuL^3(bdt)]	9.9
[CuL^4(bdt)]	12.5
[ZnL^1(bdt)]	3.8
[ZnL^2(bdt)]	>100
[ZnL^3(bdt)]	19.2
[ZnL^4(bdt)]	35.2
Rifampicin	0.1

4.2.4. Antimycobacterial assay

The activity of the complexes against *M. tuberculosis* virulent strain H37Rv was determined. The minimum inhibitory concentration (MIC) against *M. tuberculosis* was determined and results are presented in Table 9. The lowest MIC values of $-NO_2$ group containing complexes were more active against H37Rv strain than the other complexes. The highest MIC was found for the unsubstituted group containing Cu(II) and Zn(II) complexes. On the other hand, the least active complexes were the unsubstituted Cu(II) and Zn(II) complexes, which exhibited MIC > 100 μg/mL. Although the complexes have not shown better antitubercular activity than the other substituted ($-NO_2$, $-OH$ and $-OCH_3$) complexes, in general all of the complexes exhibited good activity and, except unsubstituted group complexes, all of them were less active than the standards.

5. Conclusions

Few new copper(II) and zinc(II) complexes of the type [ML(bdt)], [L = Schiff base derived from the condensation of 3-(3-phenyl-allylidene)-pentane-2,4-dione and *para* substituted aniline(X); X = $-NO_2$ (L^1), $-H$ (L^2), $-OH$ (L^3) and $-OCH_3$ (L^4); bdt = benzene-1,2-dithiol] have been synthesized and structurally characterized. They have adopted square-planar geometry around the central metal ion. Mechanistic investigations show a major groove binding for the synthesized complexes with DNA. Chemical nuclease activity of the synthesized copper complexes in the presence of an oxidizing agent, hydrogen peroxide *via* mechanistic pathway involves the formation of hydroxyl radical as the reactive species. Pathways involving singlet oxygen in the DNA photocleavage reactions have been proposed from the observation of the complete inhibition of the cleavage in the presence of sodium azide and enhancement of cleavage in D_2O. Hydroxyl radical scavengers like DMSO do not show any significant effect in the DNA cleavage activity. This result suggests the formation of singlet oxygen as the reactive species in a type-II process. The hydrolytic cleavage of DNA by the zinc complexes is supported by the evidence from free radical quenching and T4 ligase ligation. The antitumor and *in vitro* cytotoxic activities of synthesized complexes have been examined. The results suggest that all the complexes produce a potent anti-tumor and cytotoxic effect against EAC. All of the complexes exhibit good antimycobacterial activity except unsubstituted group complexes.

6. Experimental protocols

6.1. Materials and methods

All reagents and chemicals were procured from Merck products. Solvents used for electrochemical and spectroscopic studies were purified by standard procedures [56]. DNA was purchased from Bangalore Genei (India). Agarose (molecular biology grade), ethidium bromide (EB) were obtained from Sigma (USA). Tris (hydroxymethyl)aminomethane–HCl (Tris–HCl) buffer solution was prepared using deionized, sonicated triply distilled water.

6.2. Physical measurement

Carbon, hydrogen and nitrogen analysis of the complexes were carried out on a CHN analyzer Calrlo Erba 1108, Heraeus. The infrared spectra (KBr discs) of the samples were recorded on a Perkin–Elmer 783 series FTIR spectrophotometer. The electronic absorption spectra in the 200–1100 nm were obtained on a Shimadzu UV-1601 spectrophotometer. ^{1}H and ^{13}C NMR spectra (300 MHz) of the ligands and their zinc complexes were recorded on a Bruker Avance DRX 300 FT-NMR spectrometer using $CDCl_3$ and DMSO-d_6 as solvents respectively. Tetramethylsilane was used as internal standard. Fast atomic bombardment mass spectra (FAB-MS) were obtained using a VGZAB-HS spectrometer in a 3-nitrobenzylalcohol matrix. The X-band EPR spectra of the complexes were recorded at RT (300 K) and LNT (77 K) using DPPH as the g-marker. Molar conductance of 10^{-3} M solutions of the complexes in N,N′-dimethylformamide (DMF) were measured at room temperature with a Deepvision Model-601 digital direct reading deluxe conductivity meter. Magnetic susceptibility measurements were carried out by employing the Gouy method at room temperature on powder sample of the complexes. $CuSO_4 \cdot 5H_20$ was used as calibrant. Electrochemical measurements were performed on a CHI620C electrochemical analyzer with three electrode system of a glassy electrode as the working electrode, a platinum wire as auxiliary electrode and Ag/AgCl as the reference electrode. Solutions were deoxygenated by purging with N_2 prior to measurements. The metal contents of the complexes were determined according to the literature method [57]. The purity of ligands and their complexes were evaluated by column and thin layer chromatography.

6.3. Synthesis of complexes

To a stirred ethanol solution of the Schiff base(s) (5 mmol), a solution of copper(II)/zinc(II)chloride (5 mmol) in ethanol was added dropwise. After the reaction for 1 h at 70 °C, a solution of bdt (5 mmol) in ethanol was added. The reaction solution was refluxed for 2 h. After cooling the reaction mixture to an ambient temperature, the formed solid was filtered, washed with diethyl ether and finally dried in vacuum.

[CuL^1(bdt)]. Yield: 42%. IR (KBr pellet, cm^{-1}): 1612 ν(−C═N); 1576 ν(−HC═C); 1058ν(−C−S ring str.; bdt); 1476, 1322, 861 ν (−C−N str; $-NO_2$); 432 (M−N); 386 (M−S). MS m/z (%): 659 $[M + 1]^+$. Anal. Calc. for $C_{32}H_{26}N_4O_4CuS_2$: Cu, 9.7; C, 58.4; H, 4.0; N, 8.5; S, 9.7; Found: Cu, 9.5; C, 58.0; H, 4.0; N, 8.2; S, 9.5 (%). Λ_M 10^{-3} (ohm^{-1} cm^2 mol^{-1}) = 5.0 λ_{max} in DMF (cm^{-1}), 38759, 24213, 23041, 17035, 14684. μ_{eff} (BM): 1.94.

[CuL^2(bdt)]. Yield: 51%. IR (KBr pellet, cm^{-1}): 1619 ν(C═N); 1584 ν(−HC═C); 1076 ν(C−S ring str.; bdt); 441 (M−N); 394 (M−S). MS m/z (%): 567 $[M + 1]^+$. Anal. Calc. for $C_{32}H_{26}N_2CuS_2$: Cu, 11.2; C, 67.9; H, 4.6; N, 5.0; S, 11.3; Found: Cu, 11.0; C, 67.5; H, 4.5; N, 4.7 (%). Λ_M 10^{-3} (ohm^{-1} cm^2 mol^{-1}) = 7.0 λ_{max} (cm^{-1}) in DMF, 38314, 24390, 23310, 16992, 14771. μ_{eff} (BM): 1.9.

[CuL^3(bdt)]. Yield: 38%. IR (KBr pellet, cm^{-1}): 1621 ν(−C═N); 1570 ν(−HC═C); 1068 ν(−C−S ring str.; bdt); 3432 ν(−OH); 430 (M−N); 382 (M−S). MS m/z (%): 599 $[M + 1]^+$. Anal. Calc. for $C_{32}H_{26}N_2O_2CuS_2$: Cu, 10.6; C, 64.3; H, 4.4; N, 4.7; S, 10.7; Found: Cu, 10.4; C, 64.0; H, 4.2; N, 4.5; S, 10.4 (%). Λ_M 10^{-3} (ohm^{-1} cm^2 mol^{-1}) = 3.3. λ_{max} (cm^{-1}) in DMF, 38023, 24876, 23866, 16978, 14815. μ_{eff} (BM): 1.84.

[CuL^4(bdt)]. Yield: 49%. IR (KBr pellet, cm^{-1}): 1615 ν(−C═N); 1587 ν(−HC═C); 1283, 1085, ν(−C−O−C−); 1095 ν(−C−S ring str.; bdt); 429 (M−N); 397 (M−S). MS m/z (%): 629 $[M + 1]^+$. Anal. Calc. for $C_{34}H_{32}N_2O_2CuS_2$: Cu, 10.1; C, 65.0; H, 5.1; N, 4.5; S, 10.2; Found: Cu, 9.8; C, 64.7; H, 5.0; N, 4.2; S, 10.0 (%). Λ_M 10^{-3} (ohm^{-1} cm^2 mol^{-1}) = 7.3. λ_{max} (cm^{-1}) in DMF, 37453, 24331, 23585, 16949, 14793, μ_{eff} (BM): 1.89.

[ZnL^1(bdt)]. Yield: 47%. IR (KBr pellet, cm^{-1}): 1610 ν(−C═N); 1580 ν(−HC═C); 1096 ν(−C−S ring str.; bdt); 1478, 1321, 861 ν (−C−N str; $-NO_2$); 431 (M−N); 379 (M−S). ^{1}H NMR (δ): (aromatic) 6.8–7.2 (m); ($-CH_3$, 6H), 2.3 (s). ^{13}C NMR (δ): 125.0–127.6 (C_1 to C_6 and C_{13}); 136.0 (C_7); 129 (C_8); 154.6 (C_9); 18.8 (C_{10}); 152.3 (C_{11}); 121.8 (C_{12}); 146.5 (C_{14}); 125.8, 129.7, 132.7 (C_{15}, C_{16}, C_{17}, bdt). MS m/z (%): 661 $[M + 1]^+$. Anal. Calc. for $C_{32}H_{26}N_4O_4ZnS_2$: Zn, 9.9; C, 58.2; H, 4.0; N, 8.5; S, 9.7; Found: Zn, 9.7; C, 57.9; H, 4.0; N, 8.2; S, 9.4 (%). Λ_M 10^{-3} (ohm^{-1} cm^2 mol^{-1}) = 9.9. λ_{max} (cm^{-1}) in DMF, 38810, 24412, 23068. μ_{eff} (BM): diamagnetic.

[ZnL^2(bdt)]. Yield: 42%. IR (KBr pellet, cm^{-1}): 1616 ν(−C═N); 1585 ν(−HC═C); 1089 ν(−C−S ring str.; bdt); 427 (M−N); 372 (M−S).^{1}H NMR (δ): (aromatic) 6.8–7.2 (m); ($-CH_3$, 6H), 2.6 (s). ^{13}C NMR (δ): 125.5–128.0 (C_1 to C_6 and C_{13}); 137.0 (C_7); 129.1 (C_8); 152.0 (C_9); 17.5 (C_{10}); 148.4 (C_{11}); 121.0 (C_{12}); 130.0 (C_{13}); 126.8, 129.7, 133.7 (C_{15}, C_{16}, C_{17}, bdt). MS m/z (%): 569 $[M + 1]^+$. Anal. Calc. for $C_{32}H_{26}N_2ZnS_2$: Zn, 11.5; C, 67.7; H, 4.6; N, 4.9; S, 11.3; Found: Zn, 11.2; C, 67.4; H, 4.5; N, 4.7; S, 11.0 (%). Λ_M 10^{-3} (ohm^{-1} cm^2 mol^{-1}) = 5.7 λ_{max}(cm^{-1}) in DMF, 38365, 24395, 23318. μ_{eff} (BM): diamagnetic.

[ZnL^3(bdt)]. Yield: 48%. IR (KBr pellet, cm^{-1}): 1619 ν(−C═N); 1574 ν(−HC═C); 1085 ν(−C−S ring str.; bdt); 3432 ν(−OH); 435 (M−N); 391 (M−S). ^{1}H NMR (δ): (aromatic) 6.8–7.4 (m); ν(−OH, 1H), 11.7; ($-CH_3$, 6H), 2.3 (s). ^{13}C NMR (δ): 125.1–129.0 (C_1 to C_6); 137.0 (C_7); 129.0 (C_8); 152.2 (C_9); 14.5 (C_{10}); 13.0 (C_{11}); 123.6 (C_{12}); 120.3 (C_{13}); 152.4 (C_{14}); 127.5, 129.9, 134.5 (C_{15}, C_{16}, C_{17}, bdt). MS m/z (%): 601 $[M + 1]^+$. Anal. Calc. for $C_{32}H_{26}N_2O_2ZnS_2$: Zn, 10.9; C, 64.1; H, 4.4; N, 4.7; S, 10.7; Found: Zn, 10.7; C, 63.8; H, 4.4; N, 4.3; S, 10.4 (%). Λ_M 10^{-3} (ohm^{-1} cm^2 mol^{-1}) = 4.7. λ_{max} (cm^{-1}) in DMF, 38046, 24895, 23871. μ_{eff} (BM): diamagnetic.

[ZnL^4(bdt)]. Yield: 53%. IR (KBr pellet, cm^{-1}): 1621 ν(−C═N); 1587 ν(−HC═C); 1283, 1085 ν(−C−O−C−); 1105 ν(−C−S ring str.; bdt); 439 (M−N); 398 (M−S).^{1}H NMR (δ): (aromatic) 7.0–7.4 (m); ($-OCH_3$, 6H), 3.6(s); ($-CH_3$, 6H), 2.3 (s). ^{13}C NMR (δ): 125.0–128.0 (C_1 to C_6); 137.0 (C_7); 128.6 (C_8); 150.2 (C_9); 16.8 (C_{10}); 141.6 (C_{11}); 123.2 (C_{12}); 116.3 (C_{13}); 154.5 (C_{14}); 59.4 (C_{15}); 127.7, 130.0, 134.8 (C_{15}, C_{16}, C_{17}, bdt). MS m/z (%): 631 $[M + 1]^+$. Anal. Calc. for $C_{34}H_{32}N_2O_2ZnS_2$: Zn, 10.4; C, 64.8; H, 5.1; N, 4.5; S, 10.2; Found: Zn, 10.0; C, 64.2; H, 5.0; N, 4.2; S, 10.0 (%). Λ_M 10^{-3} (ohm^{-1} cm^2 mol^{-1}) = 8.3. λ_{max} (cm^{-1}) in DMF, 37458, 24335, 23582. μ_{eff} (BM): diamagnetic.

6.4. DNA binding studies

All the experiments involving the interaction of the complexes with Calf thymus (CT) DNA were carried out in Tris–HCl buffer (50 mM Tris–HCl, pH 7.2) containing 5% DMF at room temperature. A solution of CT DNA in the buffer gave a ratio of UV absorbance at 260 and 280 nm of about 1.89:1, indicating the CT DNA sufficiently free from protein. The CT DNA concentration per nucleotide was

determined by absorption spectroscopy using the molar absorption coefficient of 6600 M^{-1} cm^{-1} at 260 nm [58].

6.4.1. Absorption spectroscopic studies

Absorption titration experiments were performed by maintaining the metal complex concentration as constant at 50 μM while varying the concentration of the CT DNA within 40–400 μM. While measuring the absorption spectrum, equal quantity of CT DNA was added to both the complex solution and the reference solution to eliminate the absorbance of CT DNA itself. From the absorption data, the intrinsic binding constant K_b was determined from the plot of [DNA]/($\varepsilon_a - \varepsilon_f$) vs. [DNA] using the following equation:

$$[DNA]/\left(\varepsilon_a - \varepsilon_f\right) = [DNA]/\left(\varepsilon_b - \varepsilon_f\right) + \left[K_b\left(\varepsilon_b - \varepsilon_f\right)\right]^{-1}$$

where [DNA] is the concentration of CT DNA in base pairs. The apparent absorption coefficients ε_a, ε_f and ε_b correspond to A_{obsd}/[M], the extinction coefficient for the free metal(II) complex and extinction coefficient for the metal(II) complex in the fully bound form, respectively [59]. K_b is given by the ratio of slope to the intercept.

6.4.2. Electrochemical methods

Cyclic voltammetry and Differential pulse voltammogram studies were performed on a CHI620C electrochemical analyzer with three electrode system of glassy carbon as the working electrode, a platinum wire as auxiliary electrode and Ag/AgCl as the reference electrode. Solutions were deoxygenated by purging with N_2 prior to measurements. The freshly polished glassy electrode was modified by transferring a droplet of 2 μL of 2.5×10^{-3} M of CT DNA solution on to the surface, followed by air drying. Then the electrode was rinsed with distilled water. Thus, a CT DNA-modified glassy carbon electrode was obtained.

6.4.3. Viscosity measurements

Viscosity experiments were carried on an Ostwald viscometer, immersed in a thermostated water-bath maintained at a constant temperature at 30.0 ± 0.1 °C. CT DNA samples of approximately 0.5 mM were prepared by sonicating in order minimize complexities arising from CT DNA flexibility [60]. Flow time was measured with a digital stopwatch three times for each sample and an average flow time was calculated. Data were presented as $(\eta/\eta^0)^{1/3}$ *versus* the concentration of the metal(II) complexes, where η is the viscosity of CT DNA solution in the presence of complex, and η^0 is the viscosity of CT DNA solution in the absence of complex. Viscosity values were calculated after correcting the flow time of buffer alone (t_0), $\eta = (t - t_0)/t_0$ [61].

6.5. Nuclease activity

The extent of cleavage of super coiled (SC) pUC19 DNA (33.3 μM, 0.2 μg) to its nicked circular (NC) form was determined by agarose gel electrophoresis in 50 mM Tris–HCl buffer (pH 7.2) containing 50 mM NaCl. For photo-induced DNA cleavage studies, the reactions were carried out under illuminated conditions using UV sources at 360 nm. After exposure to light, each sample was incubated for 1 h at 37 °C and analyzed for the photo-cleaved products using gel electrophoresis as discussed below. The inhibition reactions for the "chemical nuclease" reactions were carried out under dark condition by adding reagent distamycin (50 μM)/DMSO (4 μL), prior to the addition of the each complex and the oxidizing agent hydrogen peroxide. The inhibition reactions for the photo-induced DNA were carried out at 360 nm using reagents NaN_3 (100 μM)/DMSO (4 μL) prior to the addition of the each complex. For the D_2O experiment, the solvent was used for the dilution of the sample to 18 μL. The sample after incubation for 1 h at 37 °C in a dark chamber was added to the loading buffer containing 0.25% bromophenol blue, 0.25% xylene cyanol, 30% glycerol (3 μL) and the solution was finally loaded on 0.8% agarose gel containing 1 μg/mL ethidium bromide. Electrophoresis was carried out in a dark chamber for 3 h at 50 V in Tris–acetate–EDTA buffer. Bands were visualized by UV light and photographed.

6.6. Hydrolytic DNA cleavage experiment

The 25 μL total volume of mixture of 77 μM pUC19 DNA with zinc complexes of 50 μM in 50 mM Tris–HCl buffer (pH 7.2) containing 50 mM NaCl was incubated for 30 min at 37 °C. To eliminate the effect of the oxidative species which results from the oxygen dissolved in the solution on the hydrolysis reactions, the incubation of all samples was performed under anaerobic conditions such as deoxygenated and highly purified water, isolation of air, and in nitrogen atmosphere. The hydrolytic reactions were quenched by the addition of 4 μL TBE (89 mM Tris, 89 mM boron hydroxide, 2 mM EDTA) sample buffer containing xylene cyanol and bromophenol blue. The electrophoresis of DNA cleavage products was performed on 0.8% agarose gel. The gels were run at 50 V for 45 min in 0.01 M pH 7.2 NaH_2PO_4 and Na_2HPO_4 buffer. To perform simple kinetic analysis, the electrophoresis bands were visualized by staining in an ethidium bromide solution and photographed on UV transilluminator at 360 nm.

6.7. Ligation experiment on the DNA by zinc complexes

First, the linear DNA was isolated from the pUC 19 DNA cleavage products provided by zinc complexes. Then in each parallel experiment, the 25 μL total volume of mixture containing 2 μL ligation buffer, 1 μL 0.1 M ATP, 4 μL 40% PEG, and 3 Weiss units T4 DNA ligase reacted with the linear DNA for 24 h at room temperature. The ligation products were monitored by the electrophoresis and visualized by staining in an ethidium bromide solution.

6.8. Antitumor activity

6.8.1. Animals

Adult Swiss female albino mice (20–25 g) were procured from Animal house, Vivekananda College of Pharmacy, Trichengodu, Tamil Nadu, India and used throughout the study. They were housed in microlon boxes in controlled environment (temperature 25 ± 2 °C and 12 h dark/light cycle) with standard laboratory diet and water *ad libitum*. The experiments were performed in accordance with guidelines established by the European community for the care and use of laboratory animals, and were approved by the Institutional Animal Ethics Committee (IAEC) of Vivekananda College of Pharmacy, Tamil Nadu, India.

6.8.2. Cells

EAC cells were obtained through the courtesy of Amala Cancer Research Centre, Trissur, India. They were maintained by weekly intraperitoneal inoculation of 10^6 cells/mouse [62].

6.8.3. Effect of Cu(II) and Zn(II) complexes on survival time [63]

Animals were inoculated with 1×10^6 cells/mouse on day '0' and treatment with synthesized complexes started 24 h after inoculation, at a dose of 100 mg/kg/day, p.o. The control group was treated with the same volume of 0.9% sodium chloride solution. All the treatments were given for nine days. The median survival time (MST) of each group, consisting of 10 mice was noted. The

antitumor efficacy of complexes was compared with that of 5-fluorouracil (Dabur Pharmaceutical Ltd, India; 5-FU, 20 mg/kg/day, i.p. for 9 days).

6.8.4. Effect of Cu(II) and Zn(II) complexes on hematological parameters [63]

In order to detect the influence of complexes on the hematological status of EAC-bearing mice, a comparison was made among three groups (n = 5) of mice on the 14th day after inoculation. The groups comprised of (1) tumor-bearing mice (2) tumor-bearing mice treated with complexes (100 mg/kg/day, p.o. for the first 9 days) and (3) control mice (normal). Blood was drawn from each mouse by the retro orbital plexus method and the white blood cell count (WBC), red blood cell count (RBC), hemoglobin, protein and packed cell volume (PCV) were determined [64–66].

6.8.5. Effect of Cu(II) and Zn(II) complexes on in vitro cytotoxicity

Short-term cytotoxicity was assessed by incubating 1×10^6 EAC cells in 1 mL phosphate buffer saline with varying concentrations of the complexes at 37 °C for 3 h in CO_2 atmosphere ensured using a McIntosh field jar. The viability of the cells was determined by the trypan blue exclusion method [67].

6.8.6. Effect of Cu(II) and Zn(II) complexes on human cancer cell lines by MTT assay

Human cervical cancer cell lines (HeLa), Human laryngeal epithelial cancer (Hep2), Human liver cancer (HepG2) and Human breast cancer (MCF-7) cells were obtained from National Centre for Cell Science (Pune, India). Stock cells of HeLa, Hep2, HepG2 and MCF-7 cell lines were cultured in RPMI-1640 or DMEM supplemented with 10% in activated new born calf serum, penicillin (100 IU/mL), streptomycin (100 μg/mL), and amphotericin-B (5 μg/mL) under a humidified atmosphere of 5% CO_2 at 37 °C until confluent. The cells were dissociated in 0.2% trypsin, 0.02% EDTA in phosphate buffer saline solution. The stock culture was grown in 25 cm^2 tissue-culture flasks, and cytotoxicity experiments were carried out in 96-well microtiter plates (Tarsons India, Kolkata, India).

Cell lines in the exponential growth phase were washed, trypsinized and resuspended in complete culture media. Cells were plated at 10,000 cells/well in 96-well microtiter plates and incubated for 24 h, during which a partial monolayer formed. They were then exposed to various concentrations of the complexes (0.1–100 μg/mL) and cisplatin. Control wells received only maintenance medium. The plates were incubated at 37 °C in a humidified incubator with 5% CO_2 for a period of 72 h at the end of 72 h, viability was determined by MTT assay.

6.8.7. Statistical analysis

All values were expressed as mean + SEM. The data were statistically analyzed by one-way ANOVA followed by Dunnett's test, the data of hematological parameters were analyzed using ANOVA followed by Tukey multiple comparison test. P values <0.05 were considered significant.

6.9. Antimycobacterial assay

Antimycobacterial assay was performed using microplate Alamar blue assay [68] (MABA). Suspension of *M. tuberculosis* H37Rv strain was prepared at a concentration of 10^5 cells/mL. Samples were dissolved in dimethylsulfoxide (DMSO) and subsequent dilutions were performed in 0.1 mL of 7H9 medium in the microplate together with the complexes (concentration 0.78–100 μg/mL). The plates were incubated at 37 °C for 7 days. At day 7 of incubation, 20 μL of Alamar blue solution were added to the control well. If the dye turned pink, indicating bacterial growth, the dye was then added to all remaining wells in the plate. The results were read on the following day and Minimum Inhibitory Concentration (MIC) values of the complexes were calculated. Rifampicin was used as positive control.

Acknowledgements

The authors express their heartfelt thanks to the Department of Science and Technology, New Delhi for financial assistance. They also express their gratitude to the College Managing Board, VHNSN College, Virudhunagar for providing research facilities.

References

[1] M. Coluccia, G. Natile, Anti Canc. Agents Med. Chem. 7 (2007) 111–123.
[2] P. Heffeter, U. Jungwirth, M. Jakupec, C. Hartinger, M. Galanski, L. Elbling, M. Micksche, B. Keppler, W. Berger, Drug Resist. Updat. 11 (2008) 1–16.
[3] I. Kostova, Recent Pat. Anti-Cancer Drug Discov. 1 (2006) 1–22.
[4] J. Reedijk, Med. Inorg. Chem. 93 (2005) 80–109.
[5] M. Abdul Alim Al-Bari, A. Khan, B.M. Rahman, M. Kwdrat-E-Zahan, M. Asik Mossadik, M. Anwar Ul Islam, Res. J. Agr. Biol. Sci. 3 (2007) 599–604.
[6] V. Cepeda, M.A. Fuertes, J. Castilla, C. Alonso, C. Queredo, J.M. Perez, Anti Canc. Agents Med. Chem. 7 (2007) 3–18.
[7] C. Liu, M. Wang, T. Zhang, H. Sun, Coord. Chem. Rev. 248 (2004) 147–168.
[8] A. Sreedhara, A. Cowan, J. Biol. Inorg. Chem. 6 (2001) 337–347.
[9] E.S. Raper, Coord. Chem. Rev. 61 (1985) 115–184.
[10] I.G. Dance, Polyhedron 5 (1986) 1037–1104.
[11] P.G. Blower, J.R. Dilworth, Coord. Chem. Rev. 76 (1987) 121–185.
[12] B. Krebs, G. Henkel, Angew. Chem. Int. Ed. Engl. 30 (1991) 769–788.
[13] J.R. Dilworth, J. Hu, Adv. Inorg. Chem. 40 (1993) 411–459.
[14] E.S. Raper, Coord. Chem. Rev. 153 (1996) 199–255.
[15] E.S. Raper, Coord. Chem. Rev. 165 (1997) 475–567.
[16] R.H. Holm, E.I. Solomon, Chem. Rev. 96 (1996) 2239–2314.
[17] P.T.R. Rajagopalan, A. Datta, D. Pei, Biochemistry 36 (1977) 13910–13918.
[18] C.S. Mullins, C.A. Grapperhaus, B.C. Frye, L.H. Wood, A.J. Hary, R.M. Buchanan, M.S. Mashuta, Inorg. Chem. 48 (2009) 9974–9976.
[19] H.J. Kruger, G. Peng, R.H. Holm, Inorg. Chem. 30 (1991) 734–742.
[20] G. Henkel, B. Krebs, Chem. Rev. 104 (2004) 801–824.
[21] C.F. Shaw, Chem. Rev. 99 (1999) 2589–2600.
[22] T.C. Markello, I.M. Bernardeni, W.A.N. Gahl, N. Engl. J. Med. 328 (1993) 1157–1162.
[23] P. Alexander, Z.M. Bacq, S.F. Cousens, M. Fox, A. Herve, J. Lazar, Radiat. Res. 2 (1955) 392–415.
[24] H.V. Aposhian, Metal Ions in Biology. Lippincott, 1960.
[25] N. Raman, R. Jeyamurugan, B. Rajkapoor, L. Mitu, J. Iranian Chem. Soc., in press.
[26] K. Nakamoto, Infrared and Raman Spectra of Inorganic and Coordination Compounds, fourth ed. Wiley, New York, 1986.
[27] A.B.P. Lever, Inorganic Electronic Spectroscopy. Elsevier, Amesterdam, 1984.
[28] D.M. Dooley, J. Rawlings, J.H. Dawson, P.J. Stephens, E. L-Andreasson, B.G. Malmstrom, H.B. Gray, J. Am. Chem. Soc. 101 (1979) 5038–5046.
[29] E.I. Solomon, J.W. Hare, H.B. Gray, Proc. Natl. Acad. Sci. U.S.A. 73 (1976) 1389–1393.
[30] N. Kitajima, in: A.G. Sykes (Ed.), Advances in Inorganic Chemistry, Academic Press, New York, 1992.
[31] R.K. Ray, G.B. Kauffman, Inorg. Chim. Acta 173 (1990) 207–214.
[32] N. Raman, R. Jeyamurugan, J. Coord. Chem. 62 (2009) 2375–2387.
[33] J.K. Barton, A.T. Danishefsky, J.M. Goldberg, J. Am. Chem. Soc. 106 (1984) 2172–2176.
[34] S.A. Tysoe, R.J. Morgan, A.D. Baker, T.C. Strekas, J. Phys. Chem. 97 (1993) 1707–1711.
[35] T.M. Kelly, A.B. Tossi, D.J. Mc Connell, T.C. Strekas, Nucleic Acids Res. 13 (1985) 6017–6034.
[36] G.R. Brubaker, J.N. Brown, M.K. Yoo, R.A. Kinsey, T.M. Kutchan, E.A. Mottel, Inorg. Chem. 18 (1979) 299–302.
[37] B. Adhikary, C.R. Lucas, Inorg. Chem. 33 (1994) 1376–1381.
[38] V.A. Bloomfield, D.M. Crothers, I. Tinocco Jr., Physical Chemistry of Nucleic Acids. Harper and Row, New York, 1974.
[39] M.J. Waring, Nature 219 (1968) 1320–1325.
[40] I. Somasundaram, M. Palaniandavar, J. Inorg. Biochem. 53 (1994) 95–108.
[41] A.E. Kaifer, A.J. Bard, J. Phys. Chem. 89 (1985) 4876–4880.
[42] M.T. Carter, M. Rodriguez, A.J. Bard, J. Am. Chem. Soc. 111 (1989) 8901–8911.
[43] L.S. Lerman, J. Mol. Biol. 3 (1961) 18–30.
[44] H.W. Zimmerman, Angew. Chem. Int. Ed. Engl. 25 (1986) 115–130.
[45] G.S. Manning, Q. Rev. Biophys. 11 (1978) 179–246.
[46] F. Liu, K.A. Meadows, D.R. McMillin, J. Am. Chem. Soc. 115 (1993) 6699–6704.
[47] L.M. Veal, R.L. Rill, Biochemistry 30 (1991) 1132–1140.
[48] M.S. Surendra Babu, K. Hussain Reddy, P.G. Krishna, Polyhedron 26 (2007) 572–580.

[49] R. Nisson, P.B. Merkel, D.R. Kearns, Photochem. Photobiol. 16 (1972) 117–124.
[50] C.C. Cheng, S.E. Rokita, C.J. Burrows, Angew. Chem. Int. Ed. Engl. 32 (1993) 277–278.
[51] S.A. Lesko, R.J. Lorentzen, Biochemistry 19 (1980) 3023–3028.
[52] A.U. Khan, J. Phys. Chem. 80 (1976) 2219–2227.
[53] V. Opletalová, J. Hartl, A. Patel, K. Palát Jr., V. Buchta, Farmaco 57 (2002) 135–144.
[54] C. Oberling, M. Guerin, Adv. Cancer Res. 2 (1954) 353–423.
[55] P.J. van Kranenburg-Voogd, H.J. Keizer, L.M. van Putten, Eur. J. Cancer 14 (1978) 153–157.
[56] J.E. Dickeson, L.A. Summers, Aust. J. Chem. 23 (1970) 1023–1027.
[57] R.J. Angellici, Synthesis and Techniques in Inorganic Chemistry. W.B. Saunders Company, 1969.
[58] J. Marmur, J. Mol. Biol. 3 (1961) 208–218.
[59] M.E. Reichmann, S.A. Rice, C.A. Thomas, P. Doty, J. Am. Chem. Soc. 76 (1954) 3047–3053.
[60] J.B. Charies, N. Dattagupta, D.M. Crothers, Biochemistry 21 (1982) 3933–3940.
[61] S. Satyanarayana, J.C. Daborusak, J.B. Charies, Biochemistry 32 (1983) 2573–2584.
[62] B.G. Tweedy, Phytopathology 55 (1964) 910–917.
[63] B.D. Clarkson, J.H. Burchenal, Prog. Clin. Cancer 1 (1965) 625–629.
[64] F.F. D'Amour, F.R. Blood, D.A. Belden, The Manual for Laboratory Work in Mammalian Physiology. The University of Chicago Press, Chicago, 1965.
[65] O.H. Lowry, N.T. Rosenbrough, A.L. Farr, J. Biol. Chem. 173 (1951) 265–275.
[66] J.V. Docie, Practical Hematology, second ed. J&A Churchill Ltd., London, 1958.
[67] K.R. Sheeja, G. Kuttan, R. Kuttan, Amala Res. Bull. 17 (1997) 73–76.
[68] L.A. Collins, S.G. Franzblau, Antimicrob. Agents Chemother. 41 (1997) 1004–1009.